

Intraoperative near-infrared fluorescence imaging and spectroscopy identifies residual tumor cells in wounds

David Holt
Ashwin B. Parthasarathy
Olugbenga Okusanya
Jane Keating
Ollin Venegas
Charuhas Deshpande
Giorgos Karakousis
Brian Madajewski
Amy Durham
Shuming Nie
Arjun G. Yodh
Sunil Singhal

Intraoperative near-infrared fluorescence imaging and spectroscopy identifies residual tumor cells in wounds

David Holt,^{a,*} Ashwin B. Parthasarathy,^b Olugbenga Okusanya,^c Jane Keating,^c Ollin Venegas,^c Charuhas Deshpande,^d Giorgos Karakousis,^d Brian Madajewski,^c Amy Durham,^e Shuming Nie,^f Arjun G. Yodh,^b and Sunil Singhal^c

^aUniversity of Pennsylvania School of Veterinary Medicine, Department of Clinical Studies, Philadelphia, Pennsylvania 19104, United States

^bUniversity of Pennsylvania, Department of Physics and Astronomy, Philadelphia, Pennsylvania 19104, United States

^cUniversity of Pennsylvania School of Medicine, Department of Surgery, Philadelphia, Pennsylvania 19104, United States

^dUniversity of Pennsylvania School of Medicine, Department of Pathology, Philadelphia, Pennsylvania 19104, United States

^eUniversity of Pennsylvania School of Veterinary Medicine, Department of Pathobiology, Philadelphia, Pennsylvania 19104, United States

^fEmory University, Departments of Biomedical Engineering and Chemistry, Atlanta, Georgia 30322, United States

Abstract. Surgery is the most effective method to cure patients with solid tumors, and 50% of all cancer patients undergo resection. Local recurrences are due to tumor cells remaining in the wound, thus we explore near-infrared (NIR) fluorescence spectroscopy and imaging to identify residual cancer cells after surgery. Fifteen canines and two human patients with spontaneously occurring sarcomas underwent intraoperative imaging. During the operation, the wounds were interrogated with NIR fluorescence imaging and spectroscopy. NIR monitoring identified the presence or absence of residual tumor cells after surgery in 14/15 canines with a mean fluorescence signal-to-background ratio (SBR) of ~ 16 . Ten animals showed no residual tumor cells in the wound bed (mean SBR < 2 , $P < 0.001$). None had a local recurrence at >1 -year follow-up. In five animals, the mean SBR of the wound was >15 , and histopathology confirmed tumor cells in the postsurgical wound in four/five canines. In the human pilot study, neither patient had residual tumor cells in the wound bed, and both remain disease free at >1.5 -year follow up. Intraoperative NIR fluorescence imaging and spectroscopy identifies residual tumor cells in surgical wounds. These observations suggest that NIR imaging techniques may improve tumor resection during cancer operations. © 2015 Society of Photo-Optical Instrumentation Engineers (SPIE) [DOI: [10.1117/1.JBO.20.7.076002](https://doi.org/10.1117/1.JBO.20.7.076002)]

Keywords: near-infrared fluorescence imaging; optical spectroscopy; intraoperative imaging; soft tissue sarcomas; surgical margins; indocyanine green fluorescence.

Paper 150141R received Mar. 10, 2015; accepted for publication Jun. 8, 2015; published online Jul. 9, 2015.

1 Introduction

Surgical resection is the most common and effective treatment for solid tumors in the United States.^{1,2} However, up to 40% of treated patients develop local cancer recurrence, primarily due to tumor cells left behind at the excision site. Patients with local recurrence have reduced 5-year survival rates and often require radiation therapy, making accurate identification of tumor margins and removal of residual cancer cells highly desirable.²⁻⁴ In this paper, we explore the use of intraoperative optical fluorescence imaging and spectroscopy with near-infrared (NIR) light as a means to characterize, identify, and remove residual tumor cells after standard cancer operations in canines and humans.

In order to prevent local recurrences, surgeons typically use intraoperative visual and tactile examination of the tumor to identify the tumor's borders.¹ Based on the location of the border, the surgeon will excise the tumor and thus define a "surgical margin." Once the specimen has been removed, the surgeon must determine if the surgical margins contain residual cancer cells ("positive" margin) or if the surgical margins are cancer-free ("negative" margin). Since the residual cancer is often microscopic, the surgeon cannot visualize or palpate it, and this leads to erroneous prediction of negative margins $\sim 50\%$ of

the time.^{2,3} In practice, surgeons can seek intraoperative consultation with pathologists, but intraoperative frozen sectioning of surgical margins presents technical challenges including tissue preparation, artifacts from freezing, cost, loss of tissue in smaller specimens to permanent section diagnosis, human error, and sampling error in large specimens.⁴

To ameliorate these issues, we and others have surmised that image guided surgery using intraoperative NIR imaging and spectroscopy of tumor cells could play a major role identifying cancer in the surgical margins.^{1,5,6} NIR optical imaging and spectroscopy have the potential to image tumors intraoperatively using both endogenous (oxy- and deoxyhemoglobin, blood flow) and exogenous [indocyanine green (ICG), quantum dots] contrast. NIR methods have several advantages over traditional techniques: they employ relatively simple instrumentation which is portable [compared to magnetic resonance imaging (MRI)/positron emission tomography (PET)]; they do not require ionizing radiation (compared to radiographs); they can have good sensitivity by employing readily available optical contrast agents; and they are cost effective. The imaging of NIR fluorescence from exogenous contrast agents, in particular, offers the possibility of visualizing tumor margins during

*Address all correspondence to: David Holt, E-mail: dholt@vet.upenn.edu

surgery. To date, the most common contrast agent for this purpose is ICG; it is FDA-approved, and it can be injected interstitially, intravenously, or applied topically,^{7,8} and has low toxicity and few side effects.⁹

Since its approval for human use, ICG has been used for a variety of applications in preclinical and clinical settings including retinal angiography,¹⁰ imaging neural vasculature,^{7,8,11} breast cancer detection,^{12,13} imaging the gastrointestinal tract,¹⁴ coronary angiography,¹⁵ detection of sentinel lymph nodes,^{16–19} and locating colorectal and pulmonary tumor metastases.^{20,21} Several recent reviews comprehensively highlight the strengths and clinical applications of NIR imaging.^{9,22–26} Recently, we employed NIR fluorescence imaging to identify tumors in a murine preclinical model and to characterize spontaneously occurring pulmonary tumors in canines.⁵ This research established that NIR fluorescence imaging identifies tumors and discriminates them from normal tissue. A significant additional finding of this work, however, was that NIR fluorescence imaging could not readily discriminate between fluorescence from tumors and fluorescence from normal tissues with inflammation.

In this contribution, we investigate “surgical margins,” a distinctly different clinical focus than our previous work;⁵ we continue, however, to use NIR fluorescence from ICG as a basis for real-time imaging of tumors “during” surgery. The long-range goal of the present investigation is to improve detection of residual cancer cells in the wound bed “after surgical resection” of tumors^{1,6} by providing quantitative visualization of microscopic disease that is easily missed by the eye. A secondary long-term goal of this research is to use NIR fluorescence imaging to discern the tumor margin and hence identify a surgical margin. Although we apply these novel intraoperative imaging and spectroscopy techniques to sarcoma surgery, these strategies are broadly applicable to most solid tumors.

Specifically, we report intraoperative imaging results from a naturally occurring, spontaneous, large animal sarcoma model ($n = 15$) that is similar to the corresponding human disease and pilot clinical results from two human subjects. In both animals and humans, ICG was injected intravenously 24 h prior to surgery. Although tumor ICG uptake is nonspecific, the dosages and time-from-injection provided excellent tumor-to-background contrast due to enhanced permeability and retention effects.⁶ Tumor and surgical margins were derived using NIR fluorescence contrast, and after standard-of-care sarcoma resection, NIR fluorescence contrast helped to detect residual tumor cells in the surgical bed that would have been missed.

2 Methods and Materials

2.1 NIR Fluorescence and Optical Imaging System

A custom NIR imaging instrument was developed in our laboratory to visualize tumors during surgery (BioVision Technologies[®], Exton, Pennsylvania).²⁷ Briefly, the device utilizes light from an air-cooled LED (SF1-740-iXF100, Edmund Optics, New Jersey, 742 nm, 46 W/m² illumination intensity) to illuminate the sample. The bright-field light reflectance was imaged onto a CCD camera (PixelLink PL-B741EU), and the sample fluorescence was separated from the reflectance via a dichroic beam splitter and was imaged onto another (similar) camera; a bandpass emission filter (JIOSF4-11276, central wavelength 832 nm, width 10 nm, Edmund Optics, New Jersey) in front of the second camera reduced light contamination. Note that this PixelLink camera uses a CMOS imaging sensor. CMOS

sensors convert photons to electrons at every pixel location and do not have any charge transfer mechanisms (e.g., as in comparable CCD sensors). Therefore, we do not have imaging “blooming” artifacts. Image acquisition was realized using the PixelLINK Capture OEM[®] software, and the fluorescence images were overlaid on the bright-field image for display. The entire system is mounted on a metal platform that can either be suspended above the surgical field via a ring stand or held by the surgeon over the surgical site using a handle adapter (BioMediCon[®], Moorestown, New Jersey). In a typical setting, ~10 to 12 bright-field and fluorescence images were captured (with a typical exposure time of ~100 ms) and averaged. The NIR fluorescence and optical imaging system was used in two contexts: (1) to image, *in vivo*, the fluorescence from the tumor before resection [e.g., Figs. 2(a), 3(a), and 4(a)] and fluorescence from the surgical wound after removal of the tumor [e.g., Figs. 2(b), 3(b), and 4(b)]; (2) to characterize tumor margins, by imaging fluorescence from the excised tumor *ex vivo* [e.g., Figs. 2(c), 3(c), and 4(c)].

2.2 NIR Fluorescence Spectroscopy System

A hand-held NIR fluorescence spectroscopy device (Spectropen, InPhotonics[®], Norwood Massachusetts) was also utilized in this investigation. This device was employed to interrogate tumors and surgical margins during surgery, as well as tissues *ex vivo* (described in Ref. 28). Briefly, the spectroscopy device was composed of illumination and detector fibers built into a cylindrical stainless steel sampling head and coupled via an FC connector to a spectrometer. Sample excitation was realized by light from a 785-nm, 100-mW continuous-wave laser diode, and detected light was directed via a longpass filter (800-nm edge wavelength) to a spectrometer (DeltaNu, Laramie, Wyoming) that computed the fluorescence spectra over a wavelength range of 800 to 930 nm with resolution of 0.6 nm. During experiments, the stainless steel sampling head was held on the surface of the investigated tissue, ensuring that the measurement geometry was constant across samples. The fixed positions of the illumination and detection fiber tips ensured that the sampling area was uniform across all measurements. We made the assumption that tissue optical properties are similar across different samples. While this assumption is not strictly true, we believe that changes in tissue optical properties within the tumor environment (i.e., in and around the tumor) are small. Finally, the illumination intensity and detector integration time were held constant across all measurements. Thus, the detected fluorescence intensity (in spectrometer counts) was directly compared across different samples and tissue types. The integration time of the spectrometer was fixed at its lowest value of 0.1 s in order to minimize saturation (an effective strategy in most but not all cases). The spectroscopy device was used to quantify the fluorescence from specific tissue regions in two situations: (1) *in vivo*, from highly fluorescent regions within the surgical margins, after tumor resection; and (2) *ex vivo*, from different spatial locations on the primary tumor, after resection.

2.3 Canine Study Design

Fifteen canines with primary soft tissue sarcomas amenable to surgical resection were recruited at the University of Pennsylvania, School of Veterinary Medicine. The study was approved by the University’s Institutional Animal Care and Use Committee.

Informed consent was obtained from all owners. At the time of surgery, a standard-of-care sarcoma resection was performed.

All dogs received 3 mg/kg IV ICG (Akorn Inc., Lake Forest, Illinois) 24 h prior to surgery. Intraoperative NIR imaging instrumentation was used to inspect the surgical site before and after sarcoma resection. The imaging devices were draped with sterile plastic and were used to image the primary tumor and the surrounding tissues in all dogs before the resection. Following resection, the imaging system was again used to confirm margins and examine tissues in the surgery site that might harbor residual cancer deposits. Finally, the imaging system was used to characterize the tumor margins *ex vivo* (described below). The hand-held NIR spectroscopy device (distinct from the imaging system) quantified fluorescence from residual cancer in the surgical wound after tumor resection (*in vivo*) when applicable and fluorescence from the tumor (*ex vivo* after resection). Any tissue in the surgery site suspected to contain residual cancer was excised and submitted separately for histopathological evaluation. Following removal of all tissues, the specimens were imaged *ex vivo* prior to submission for histopathology. A board certified veterinary staff pathologist rendered a final report on all specimens. All protocols were in compliance with the Guide for the Care and Use of Laboratory Animals.

2.4 Pilot Human Studies

Surgical resection studies were performed in two human patients after obtaining informed consent. The study was approved by the University of Pennsylvania's Institutional Review Board. Both patients received 5 mg/kg ICG intravenously 24 h before surgery. A standard resection of the sarcoma was performed on each patient and was not altered for the purposes of this study. In a procedure similar to the canine study, the entire cavity was palpated and visually inspected to identify the tumor and then the cavity along with the tumor was imaged using the NIR imaging instrumentation prior to tumor resection. Once the resection was completed, a final inspection of the surgical site was performed with the NIR fluorescence and optical imaging instrumentation to identify residual cancer cells. Potential sites of residual cancer cells were investigated with the hand-held NIR fluorescence spectrometry device and biopsies were obtained for histopathology. The resected tumors were imaged *ex vivo* using the NIR imaging system, and the fluorescence from the tumor was quantified *ex vivo* using the hand-held NIR spectrometer (distinct from the imaging system). All resected specimens were sent for histopathology.

2.5 Assessment of Primary Tumor, Tumor Margin, and Surgical Margin

All canine cases were managed using standard-of-care veterinary practices. The veterinary surgeon and assistant used visual and tactile information to identify the tumor. Three distinct measurements/experiments were performed to image/characterize the primary tumor, the surgical margin, and the tumor margin.

First, the primary tumor was imaged *in vivo* using the NIR fluorescence and optical imaging system, prior to surgical resection. ICG fluorescence from the primary tumor was also quantified using the hand-held NIR spectroscopy device. The tumor was then excised for further interrogation and histopathology.

Second, the surgical site was imaged after surgical resection using the NIR fluorescence imaging instrumentation, and it was

systemically interrogated with the hand-held NIR spectrometer probe in order to characterize the surgical margins and identify potential residual cancer cells [characterized by high fluorescence, e.g., Fig. 2(b)]. Then, the fluorescence from these regions were quantified using the hand-held NIR spectrometry probe (fluorescence spectrometry counts from these regions were typically >10,000). In such a manner, the surgical field was inspected in at least 12 locations, with measurements taken in triplicate at each location. Additional measurements were taken from locations whose signals deviated by more than 10%. Tissue biopsies were taken from areas in the surgical site with substantial fluorescence (>10,000 spectrometer counts) to confirm the presence of residual tumor cells.

Finally, in order to characterize the tumor margins, the excised tumors were reimaged *ex vivo*, using both the NIR fluorescence imaging device and the NIR handheld spectroscopy probe. In a typical resection, the surgeon excised the tumor and surrounding normal tissue (providing for a margin of error). The palpable edge of the tumor in the excised tissue was first identified and marked by the surgeon. This palpable edge defined the "tumor margin" within the excised tissue. Fluorescence measurements were obtained using the handheld NIR spectroscopic probe, in the center of the tumor and at positions 3-, 6-, 9-, and 12-o'clock around the tumor but within the tumor margin. NIR fluorescence imaging was then used to identify a "fluorescence" margin, i.e., the spatial points at the edge of the tumor with fluorescence-to-background ratio below a defined cutoff (see Secs. 3.2 and 3.3 for more details). The fluorescence in the tissue surrounding the tumor was characterized in intervals spaced every 3 mm beyond the "tumor margin." Whenever possible, biopsies were taken at each interval and were submitted for histopathology.

2.6 Histopathology and Fluorescence Microscopy

Histopathology was used to evaluate all resected tissues. All samples were fixed in 10% formalin, embedded in paraffin, sectioned, and evaluated by a Board-certified veterinary pathologist. Fluorescence microscopy was utilized to verify the accumulation of ICG within resected tissues. Five micrometer-thick sections from tissue biopsies obtained during the surgery were mounted with a glycerin-based mounting media and frozen tumor sections were prepared as previously described.²⁹ The samples were examined using an Olympus® IX51 fluorescent microscope equipped with an ICG specific filter set (Chroma® 49030). Fluorescence images were acquired using a PixeLink® NIR CCD camera (PL-B741EU). Each sample was then subsequently stained with hematoxylin and eosin and reimaged using white light. Fluorescence images were processed using ImageJ® (public domain software developed by the National Institutes of Health).³⁰ The images were overlaid on white-light images to create color-NIR images.

2.7 Monte Carlo Simulation of Fluorescence Light Transport

In order to understand and corroborate some of our experimental results, we performed computer simulations of the transport of fluorescence light from the tumor to the tissue surface, using a Monte Carlo approach based on the Monte Carlo model of steady-state light transport in multilayered tissue method.^{31,32} For these simulations, we assumed a cylindrically symmetric tissue geometry [Fig. 1(a)] with tissue surface in the $z = 0$

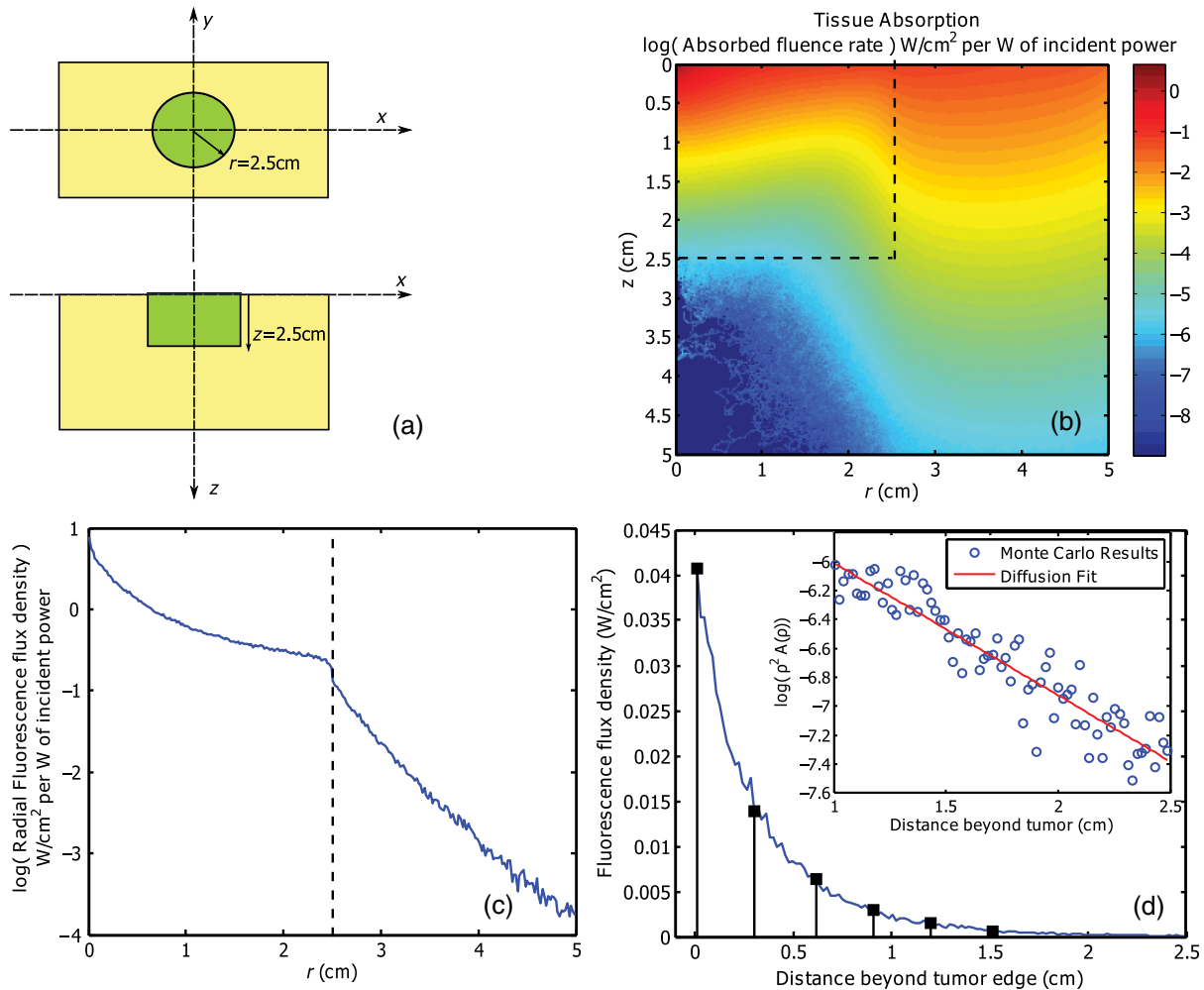


Fig. 1 Monte-Carlo simulation of light transport. (a) Schematic of tissue geometry used in the simulation. (b) Total absorbed excitation light in the tissue, expressed in a logarithmic scale. The x axis denotes radial coordinate while the y axis denotes depth. (c) Detected fluorescence on the surface of the tissue expressed as a function of radial distance from the center of the tissue. (d) Fluorescence intensity detected beyond the tumor edge (inset). Radial fluorescence intensity fit to a photon diffusion model. Linear fit denotes that the radial distribution of light fits a diffusion model.

plane. Background tissue was assumed to be homogeneous, and a tumor (5 cm diameter, 2.5 cm thick) simulating heterogeneity was located on the tissue surface. The size of this tumor heterogeneity is consistent with the average size of the excised tumors in our experiment. The optical properties of the background tissue and the tumor were calculated from assumed concentrations of oxygenated and deoxygenated hemoglobin, and ICG.^{33–35} The assumed optical properties are summarized in Table 1. Tissue absorption coefficients were calculated from these chromophore concentrations and their known spectra.³⁶ A total of 10 million excitation photons were simulated and launched into the tissue; they were distributed over a 10-cm diameter area transversely centered on the tumor (i.e., uniform collimated illumination). The paths of each photon through the tissue were tracked, and absorption of excitation light was measured in the tissue. Exploiting the cylindrical symmetry of the simulating geometry, the absorption of excited light was scored in 256×256 positions (each position represents a radial ring at a specified depth below the surface). One hundred fluorescence photons were generated from each position, and the net fluorescence exiting the tissue was recorded into 256 radial bins on the surface.

Table 1 Simulation parameters.

Chromophore	Tissue (μM)		Tumor (μM)	
	730 nm	820 nm	730 nm	820 nm
Oxyhemoglobin	42		47.25	
Deoxyhemoglobin	18		27.75	
ICG	—		3	
Tissue optical properties	Tissue		Tumor	
	730 nm	820 nm	730 nm	820 nm
Absorption coefficient (cm^{-1})	0.122	0.105	0.573	1.32
Scattering coefficient (cm^{-1})	100	75	125	93

Note: ICG, indocyanine green.

2.8 Quantification of signal-to-background ratios

The fluorescence contrast from the *in vivo* and *ex vivo* experiments were quantified by a signal-to-background ratio (SBR). In order to analyze the images obtained with the NIR fluorescence imaging instrumentation, the average fluorescence intensity within each specific region of interest (ROI) from an image was computed using the ROI plugin of ImageJ[®]. The tumor margin was identified and marked by palpation (as described previously). The “signal” was quantified as the average fluorescence from the regions identified as tumor. The “background” was identified as interstitial tissue (such as muscle, blood vessels, fat, and so on) surrounding the tumor. Our hypothesis is, although ICG is nonspecific to the tumor cells, it preferentially accumulates to a greater extent in the tumor due to the enhanced permeability and retention (EPR) effects.³⁷ Any accumulation of ICG in the surrounding tissue is not retained and is cleared over 24 h. Since an aim of this work is to characterize the tumor margins with ICG fluorescence, we make the assumption that the standard-of-care procedure of palpation accurately identifies the primary solid tumor. Note that by averaging over multiple tissue types, “background” fluorescence is less sensitive to microscopic disease beyond the palpable edge.

For a specific case, the tumor contrast was quantified as an SBR, by normalizing the average fluorescence “signal” from the tumor in that animal (or patient) with the average “background” from the surrounding tissues. In experiments involving the NIR spectrometer device, the spectrometer counts from tumor and background regions were used to derive the SBR. The mean and standard deviations of the SBRs were then computed

from SBRs computed from all animals (or patients in the human study).

Statistical significance of differences in median values of nonfluorescing versus fluorescing regions of the tumors was assessed by the Mann–Whitney test. All statistical analyses were performed in SAS Version 9.3 (SAS Institute, Inc., Cary, North Carolina).

3 Results

3.1 NIR Fluorescence Imaging Identifies Sarcomas in Canines

The first experiment used NIR ICG fluorescence to identify spontaneously occurring sarcomas in canines. Table 2 shows the distribution and characteristics of the 15 canines with sarcomas recruited for this study. Ten soft-tissue sarcomas involved either the proximal ($n = 5$) or distal parts ($n = 5$) of a limb, while three involved the thoracic ($n = 2$) or abdominal ($n = 1$) body wall. One sarcoma was located over the sacrum and one was in the right perineum. No evidence of pulmonary metastatic disease was found on thoracic radiographs in any case. No evidence of ICG toxicity was found. All 15 animals were monitored in the hospital until discharge.

Tumors were easily identified and exposed by the surgeon in all cases. Preoperative NIR imaging was unreliable unless the tumor had ulcerated through the overlying skin. This effect is likely due to the limited penetration of excitation and emission light through the skin. After the skin was removed, 14 out of 15 sarcomas fluoresced strongly in the images at the surgical site:

Table 2 Canine subject characteristics.

Subject	Breed	Histology	Tumor location	Size (cm)	Margin imaging	Margin histology	Follow-up
1	Brittany spaniel	PVWT	Shoulder	10	Negative	Negative	18 months no recurrence
2	Miniature pinscher	PVWT	Hock	1.5	Negative	Negative	20 months no recurrence
3	Mixed breed	Sarcoma	Thorax	2	Negative	Positive	25 months no recurrence
4	Labrador	Myxosarcoma	Thorax	18	Negative	Negative	11 months no recurrence
5	Labrador	Myxofibro-sarcoma	Sacrum	12	Negative	Negative	22 months no recurrence
6	Golden retriever	PVWT	Flank	16	Negative	Negative	16 months no recurrence
7	Old English sheepdog	Recurrent PVWT	Elbow	2	Positive	Positive	20 months tumor regrowth
8	Golden retriever	PVWT	Antebrachium	8	Positive	Positive	20 months no recurrence
9	Labrador	PVWT	Thigh	6	Negative	Negative	16 months no regrowth
10	Mixed breed	PVWT	Perineum	4.5	Positive	Negative	12 months, no recurrence
11	Mixed breed	PVWT	Antebrachium	4	Positive	Positive	Postoperative radiation, 8 months no recurrence
12	Mixed breed	Fibrosarcoma	Antebrachium	5	Negative	Negative	4 months no recurrence
13	Husky	Sarcoma	Carpus	4.5	Positive	Positive	2 months tumor regrowth
14	Brittany	Spindle cell sarcoma	Thigh	7	Negative	Negative	3 months no recurrence
15	Miniature pinscher	PVWT	Thigh	3	Negative	Negative	1 month no recurrence

Note: PVWT, perivascular wall tumor.

SBR 16 ± 5.1 [mean \pm standard deviation; Figs. 2(a), 3(a), and 4(a)]. Fluorescence from some tumors was strong enough to saturate the camera. The SBR was computed from the fluorescence and background images, as described earlier. The single nonresponsive case was characterized by weak tumor fluorescence. This case (#4) was a myxosarcoma; when sectioned, it was found to be comprised largely of myxomatous matrix rather than solid tumor parenchyma. We note that our instrument is only sensitive to ICG fluorescence and not tumor autofluorescence.

3.2 NIR Fluorescence Spectroscopy Measures Higher ICG Fluorescence from Tumors

The second experiment quantified ICG fluorescence and SBR from the primary tumor using the hand-held NIR fluorescence spectroscopy device. First, we measured the background fluorescence signal (at 820 nm) from normal tissues (distant from the tumor) using the hand-held NIR spectroscopy device [Fig. 5(a)]. The mean fluorescence intensity of the background structures ranged widely from 89 to 9946 spectrometer counts.

Muscle was found to have the least background fluorescence (684 ± 376 counts and full range from 89 to 1199). The fluorescence intensity from fat, blood vessels, and fascia were measured to be 5897 ± 3181 counts (range 589 to 9946), 5781 ± 2821 counts (range 217 to 8841), and 3601 ± 1741 counts (range 2215 to 6053), respectively. Thus, the average background fluorescence at 820 nm computed from background measurements from all animals and all tissues were 3991 ± 1075 counts [range 89 to 9946; Fig. 5(a)]. This average background fluorescence was used for the background in all of the SBR.

From the 14 responsive cases, the mean tumor fluorescence using the hand-held NIR spectroscopy device at 820 nm was $58,522 \pm 871$ counts. [range $> 57,046$, error in tumor fluorescence is low due to saturation of spectrometer at 60,000 counts, Fig. 6(a)]. Characterization of the variation in fluorescence intensity from the center of the tumor to the tumor edge (identified by palpation) was not possible due to signal saturation. Saturation of the tumor signal is primarily indicative of significantly higher ICG concentration within the tumor, and these saturation effects skew the SBRs to be smaller than their true

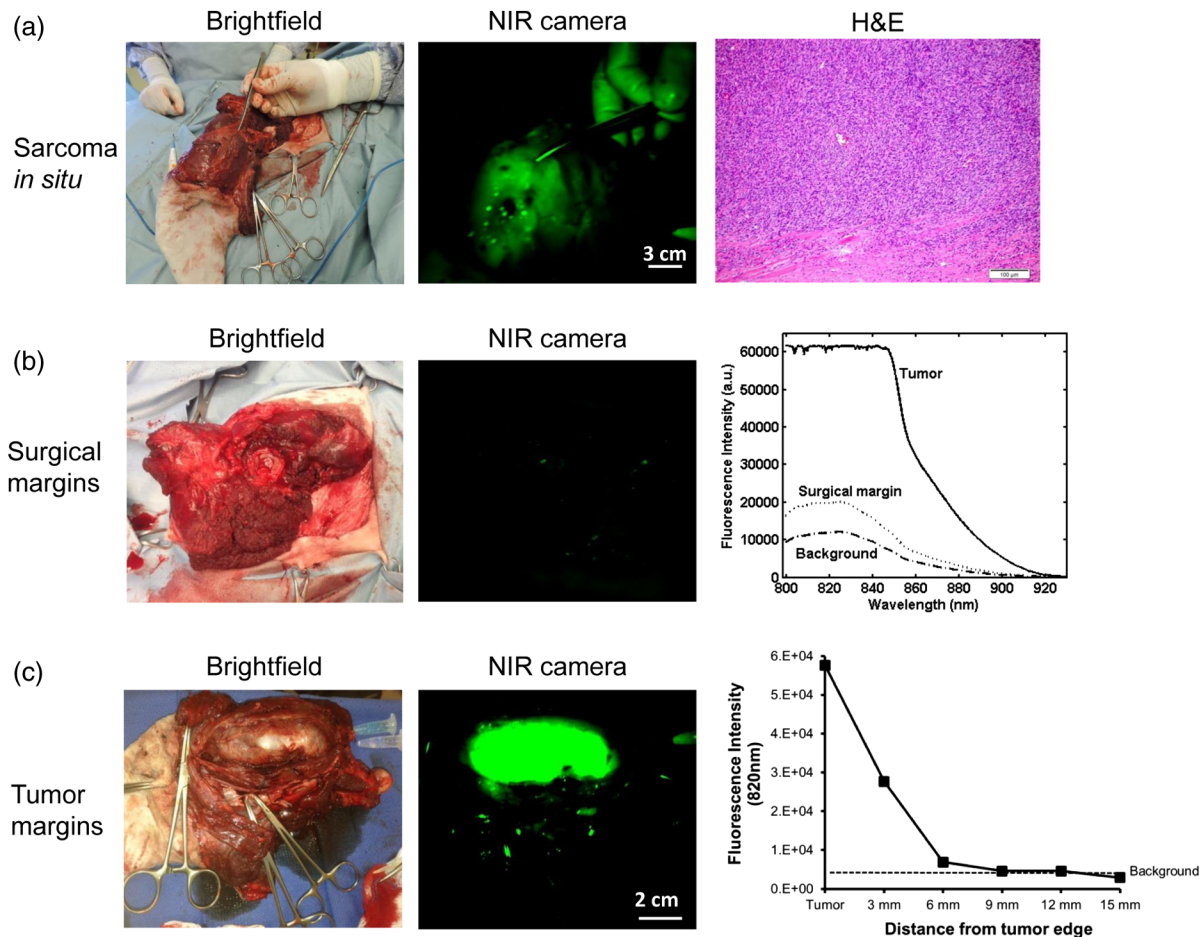


Fig. 2 Representative resection of a 7-cm perivascular wall tumor in a 17-kg Brittany spaniel. (a) The canine was injected with 3 mg/kg of indocyanine green (ICG) 24 h prior to surgery. During the operation, the tumor was fluorescent *in vivo*. Note that the surgeon's hand appears to be fluorescent because of strong reflection from the latex gloves. We have found that the use of nonlatex black gloves solves this issue. (b) After removing the sarcoma, the wound bed was examined and did not demonstrate any residual tumor cells. (c) *Ex vivo*, the tumor was fluorescent. The near-infrared (NIR) signal emitted from the sarcoma extended up to 6 mm into the surrounding tissues that did not contain microscopic evidence of tumor cells or ICG. Scale bars are approximate.

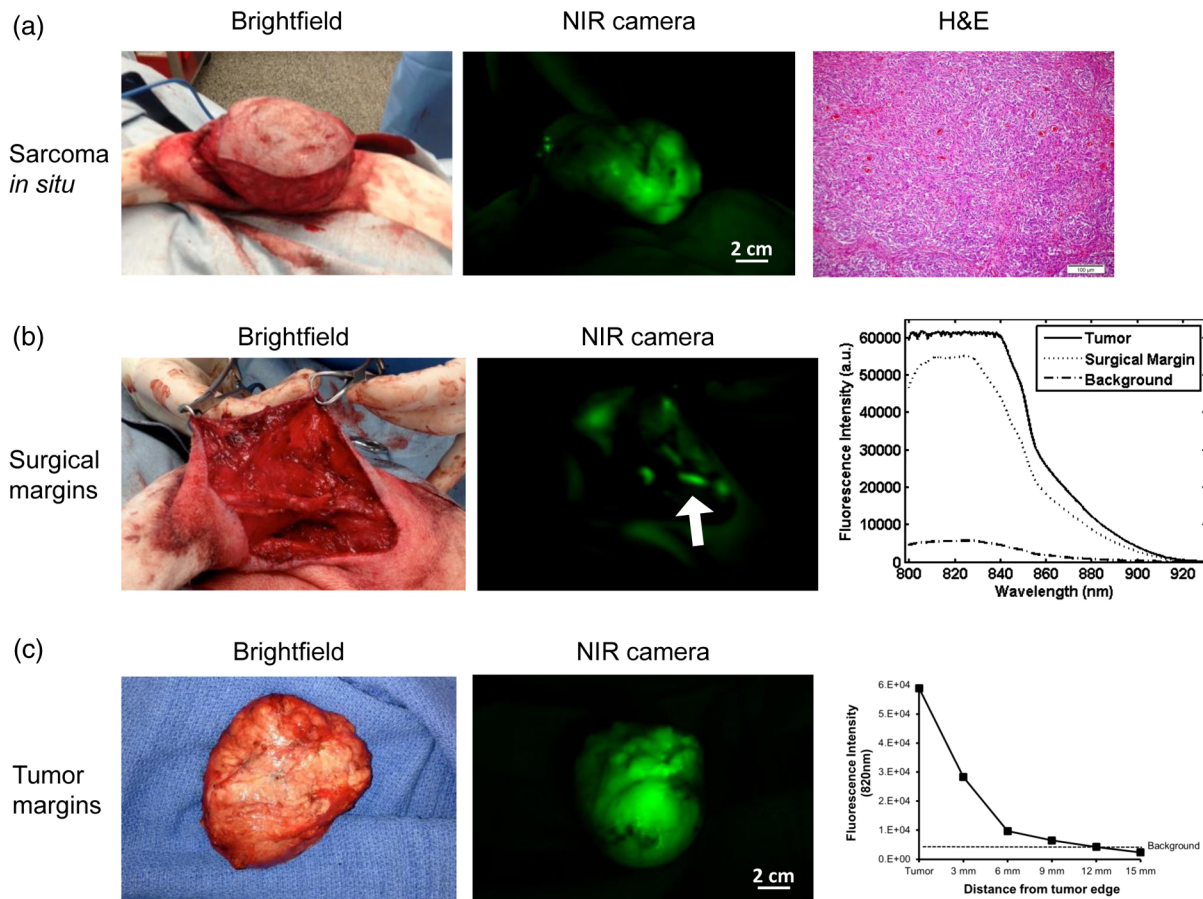


Fig. 3 Representative resection of a 4-cm sarcoma from the right antebrachium of a 13 kg mixed breed dog. (a) Again, the tumor was fluorescent *in vivo* and confirmed to be a perivascular wall tumor by H&E. (b) After removing the sarcoma, the wound bed was interrogated for residual tumor cells. Although grossly there did not appear to be cancer cells, spectroscopy and optical imaging rapidly brought attention to an area on the skin that contained a positive surgical margin. This was confirmed by pathology. (c) *Ex vivo*, the tumor was fluorescent and the NIR signal was strong throughout the entire specimen and part of the surrounding normal tissues. Scale bars are approximate.

value. The SBR of the tumor center to the surrounding tissue was computed to be 16.0 ± 5.2 (range 9.7 to 26). The SBR for the nonresponsive myxosarcoma case was 2.7.

We note that high illumination intensity was required to record an appreciable signal from the background tissue with the hand-held spectroscopy device. By collecting appreciable signals from background tissues, we prevent artificial inflation of the SBR measure. On the other hand, in four cases, the fluorescence from the tumor saturated the spectrometer even at the lowest integration times. Whereas this saturation of the signal is less than ideal, it likely indicates that the true SBR is >16 . In future iterations of the device, it should be possible to reduce saturation effects and to quantify the concentration of ICG in the sampling volume. Ratios of tumor-to-background ICG concentration will then provide a more quantitative SBR metric than the fluorescence intensity alone.

The histological subtypes of the primary tumors were the perivascular wall tumor ($n = 9$), undifferentiated sarcoma ($n = 2$), fibrosarcoma ($n = 1$), spindle cell sarcoma ($n = 1$), myxofibrosarcoma ($n = 1$), and myxosarcoma ($n = 1$). The distribution of the fluorescence from all primary tumors, as well as the surrounding tissues, is shown in Fig. 5(a). Based on this clearly bimodal distribution, a cutoff of $SBR = 5$ was established for

identification of tumors from surrounding tissue. With this definition, the NIR fluorescence clearly identified 14/15 primary sarcomas [Figs. 2(a), 3(a), and 4(a)].

3.3 NIR Fluorescence Imaging and Spectroscopy Detects Tumor Cells in Surgical Margins

NIR fluorescence imaging was utilized to visualize tissue and identify residual tumor cells after surgical resection of the primary tumor. Following resection of the primary sarcoma, the veterinary surgeon and assistant inspected the wound (i.e., the surgical site after tumor resection). In all but two cases, they decided that the sarcoma had been completely removed and were satisfied with operation's outcome. Nevertheless, regions of high fluorescence intensity, as identified from NIR fluorescence and optical imaging, were marked for further interrogation; the fluorescence from these potential sites of residual cancer was quantified with the hand-held NIR fluorescence spectrometer. The spectrometer was employed to collect fluorescence at 820 nm over at least eight different locations in the surgical wound from each animal. In every case, the most fluorescent region in the surgical wound was biopsied and stained for pathological review. The SBR was computed for all these

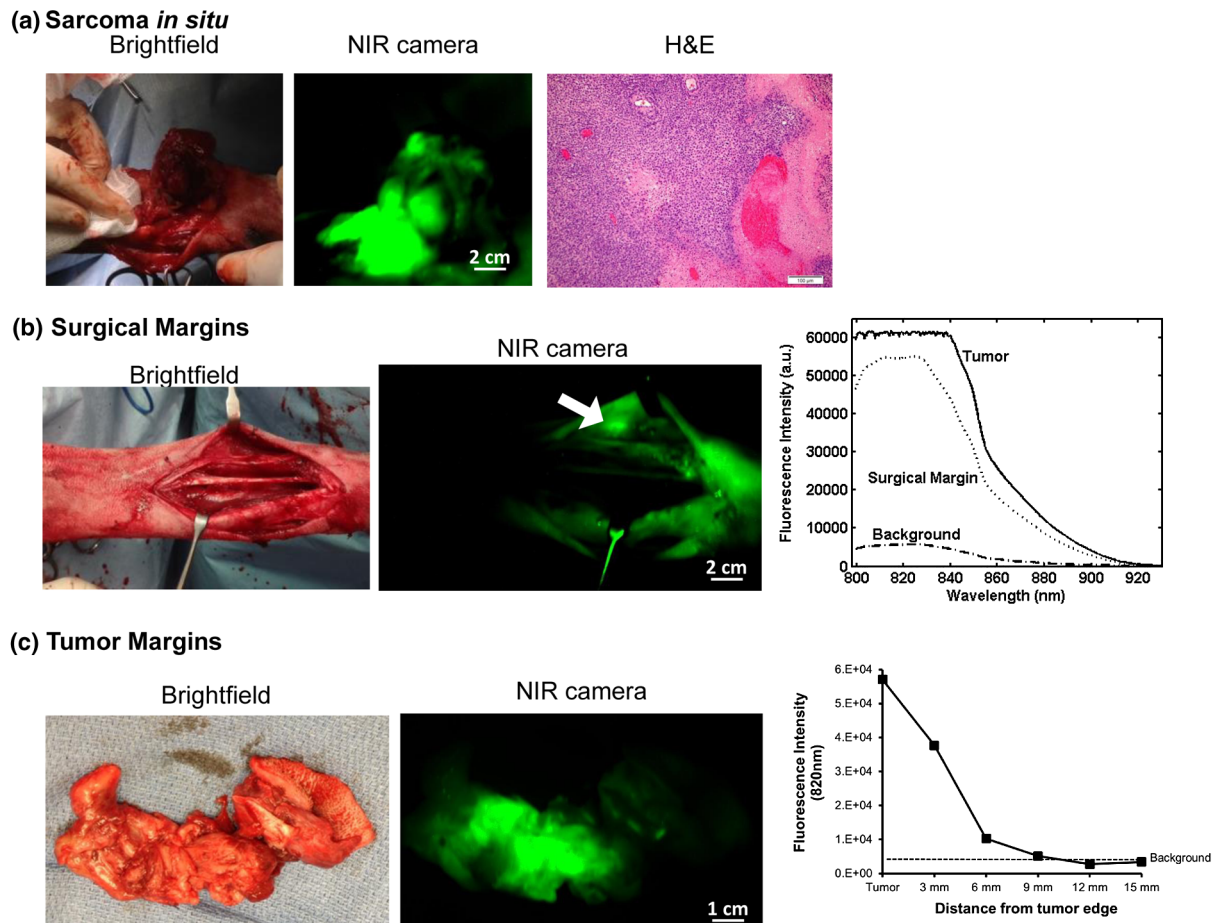


Fig. 4 Surgical removal of a 4.5-cm undifferentiated sarcoma from the right carpus of a 30 kg husky. (a) *In vivo*, the tumor was fluorescent and saturated the spectrometer and CCD imaging apparatus. (b) After removing the tumor, spectroscopy and CCD imaging identified a concerning region along the superior flap of skin, indicated by the white arrow. This tissue was biopsied and confirmed to contain residual tumor cells. Skin appears to be fluorescent due to specular reflection. Placing a blue sterile lining around the wound eliminates this background. However, visibility of the skin can be useful, because it provides context for the surgical wound in relation to canine extremities. (c) After removing the tumor, the specimen was uniformly fluorescent along the entire surgical border. Scale bars are approximate.

cases; their distribution is shown in Fig. 5(b). From this bimodal distribution, $SBR < 5$ and $SBR > 10$ were established as cutoff values for negative and positive margins. The error bars denote the deviation in fluorescence intensity and SBRs computed from different surgical cases.

In 10 animals, the surgical margin did not appear to have any residual fluorescence (negative margin) compared to the surgical wound [Fig. 2(b)] (i.e., it was characterized by $SBR < 5$). NIR fluorescence intensity at 820 nm was measured in these tissues near the margin to be 6885 ± 3804 counts [range 1476 to 11,723; Fig. 5(b)] yielding an SBR of 1.8 ± 1.4 [range 0.4 to 4.9; Fig. 5(c)]. Biopsies from the most fluorescent locations obtained from this cohort of canines found no evidence of tumor cells (i.e., the sampled tissues were true negative).

In five animals, the surgical margins exhibited areas with high fluorescence (positive margin) after tumor removal [Figs. 3(b) and 4(b)], i.e., characterized by $SBR > 10$. NIR fluorescence intensity at 820 nm was measured to be $51,546 \pm 2931$ counts [range 46,404 to 53,695; Fig. 5(b)] yielding a margin SBR of 16.3 ± 6.1 [range 10.5 to 24.3; Fig. 5(c)]. Biopsies from these locations confirmed the presence of residual tumor

in four/five of these canines (true positive). One of the canines with fluorescence from the surgical wound did not have residual tumor cells (false positive).

The data from the four canines with true positive tumor margins were interrogated further, i.e., data from canines with highly fluorescent residual tumor cells and histologically proven malignant cells. The NIR (820 nm) fluorescent intensity of the background and the margins in these cases were 3294 ± 1122 counts (range 89 to 5492) and $51,247 \pm 3295$ counts (range 46,404 to 53,695), respectively, resulting in an SBR of 17.3 ± 6.7 (range 10.5 to 24.2). Statistical analysis showed a significant difference (*t*-test, $p < 0.0001$) between the fluorescence of the surgical margins in the 10 canines with minimal fluorescence (mean 6885 a.u.) and no residual tumor cells (true negative) compared to the fluorescence of the four canines with high residual fluorescence (mean 51,247 a.u.) and histologically evident tumor cells (true positive). On histology, these positive margins contained tumor tissue that resembled the primary tumor.

The NIR fluorescent intensity (820 nm) of the background and margins in the animal with a false positive result were 4102

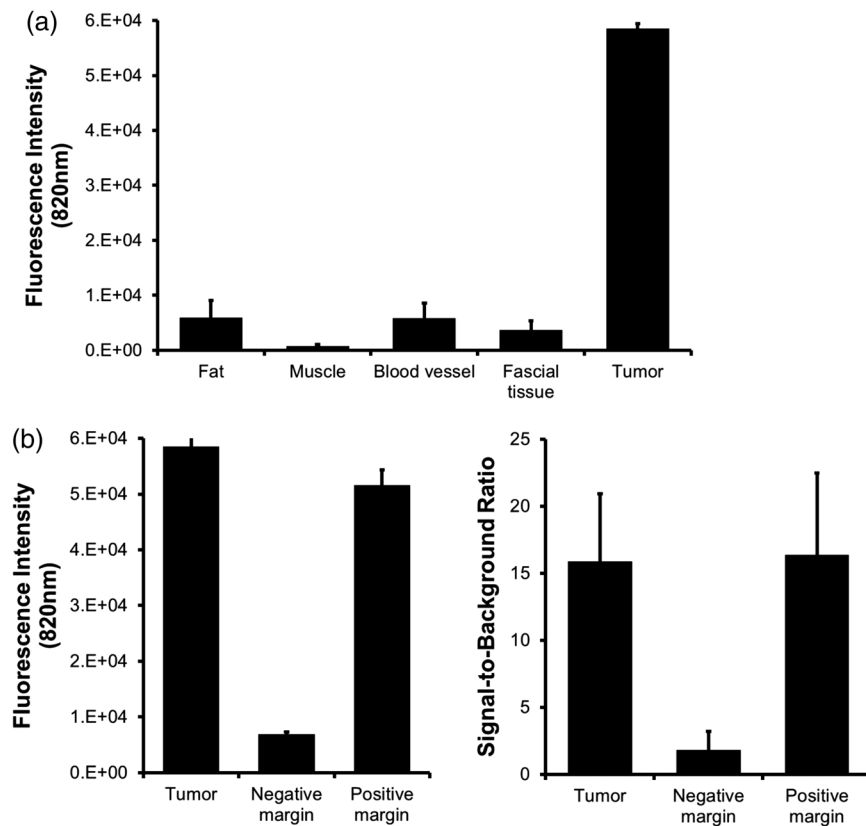


Fig. 5 (a) In 15 canine subjects, the mean fluorescence from fat, muscle, blood vessels, fascia, and the tumors were 5897 ± 3181 , 684 ± 376 , 5781 ± 2821 , 3601 ± 1741 , and $58,522 \pm 871$, respectively. (b) After removing the primary tumor, the mean fluorescence from the wound bed was dependent on the presence of residual tumor cells. In the cases with histologically proven negative margins, the mean fluorescence was 6885 ± 3804 . In the five cases with residual tumor in the wound, the mean fluorescent intensity was $51,546 \pm 2931$. The signal-to-background ratio in the wounds with the negative margins versus positive margins was 1.8 versus 16.3, respectively.

counts (range 765 to 8696) and 57,402 counts, respectively. Thus, the SBR was 12.9. Histology from biopsies obtained from this animal revealed that fluorescence was arising from an inflammatory area of congested tissue containing fibroblasts, stroma, neutrophils, macrophages, and areas of necrosis. Inflammatory tissues and organ congestion have been previously observed to have an increased uptake of ICG, an effect which could potentially explain the elevated NIR signal in this case.^{5,38}

Together, this data suggests that NIR optical fluorescence imaging and spectroscopy of the surgical wound after a sarcoma resection can identify potential areas of residual tumor cells. This is the first and arguably most significant result of this paper. In a surgical setting, with caveats about limited sample size, NIR fluorescence imaging followed by NIR fluorescence spectroscopy had an 80% positive predictive value for residual tumor cells remaining in the surgical margins. In addition, the absence of fluorescence in the surgical margin had a 100% negative predictive value.

3.4 NIR Fluorescence Imaging Overestimates Tumor Margins

Before a surgeon starts an operation, the edge of the tumor must be precisely identified and so it can be avoided. Inadvertent excisions into the tumor can sometimes result in marginal resections,

undesirable seeding of the surgical wound, and disruption of natural tissue borders.³⁹ Also, if the tumor is located close to a critical structure such as a nerve or vessel, then excessive excision around the tumor and surrounding normal tissue poses risks for injuring these important structures. Therefore, the typical excised tissue is slightly larger than the tumor margin. One objective of our study was to characterize the NIR fluorescence around the tumor margin (identified by the palpable edge), and evaluate if NIR fluorescence imaging can be used to accurately define the tumor margins.

To this end, we quantified NIR fluorescence intensity (820 nm) around the tumor margins in 10 primary sarcomas *ex vivo* using the NIR fluorescence and optical imaging instruments. The fluorescence intensity (measured *ex vivo*) averaged over the primary tumor ranged between 57,046 and 59,775 counts (mean $58,366 \pm 953$) whereas the background intensity was 2215 to 6053 counts (mean 3962 ± 1190). The average fluorescence intensity was then quantified in 3 mm intervals away from the tumor margins. The mean fluorescence intensity (at 820 nm) at 0, 3, 6, and 9 mm intervals away from the edge of the tumor were $53,656 \pm 6196$ counts, $32,262 \pm 8257$ counts, $6007 \pm 10,904$ counts, and 5572 ± 5011 counts, respectively [Figs. 2(c), 3(c), and 4(c)]. Although, the raw signal 3 mm from the palpable tumor edge was significantly different than tumor ($p = 0.02$) and background ($p = 0.01$), the NIR

fluorescence signal did not diminish to background levels until 6 mm ($p < 0.001$) from the tumor edge.

We tested three different hypotheses regarding the presence of NIR fluorescence away from the tumor margin. First, we checked if the NIR fluorescence was due to the presence of tumor cells beyond the margin. Histology from sections adjacent to the primary tumor did not show evidence of tumor cells (Fig. 6).

Our second hypothesis was that the NIR fluorescence was due to ICG that leaked beyond the tumor boundary. ICG is a small macromolecule (~ 5 nm); therefore, it can readily leak from the tumor into the surrounding tissues. Thus, circumferential biopsies around the tumor margins and away from the edge of the tumor were prepared for immunofluorescence microscopy. In 12 different samples, we did not find any ICG fluorescence particles at the 3 and 6 mm locations outside of the tumor (Fig. 6). Further, histology of these specimens showed no evidence of inflammatory infiltration or abnormal tissues.

We also analyzed the pseudocapsule around the tumor. The pseudocapsule is a 1 to 2 mm area around the primary tumor that develops due to compression of noncancerous tissue by the expanding sarcoma. This region fluoresced in a manner similar to the tumor and was technically difficult to differentiate from the tumor. Further histopathology showed that the pseudocapsule did contain ICG, and in some instances, the fluorescence was more pronounced than the underlying tumor (Fig. 6).

In principle, it is also possible that the presence of NIR fluorescence signal away from the tumor margin is tumor fluorescence light that has scattered out of the tumor and diffused through the sample, emerging outside the tumor edge. To explore this third hypothesis, we measured the fluorescence from tissues surrounding the tumor *in situ*. We then analyzed the fluorescence from fine $3 \mu\text{m}$ sections of tissues in the margins surrounding the tumor *ex situ*. We found that although

these tissues were fluorescent *in situ*, these tissues were not fluorescent when they were removed from their location (*ex situ*; Fig. 6). This observation indicates that the measured signal is the fluorescence light from the tumor regions.

In order to confirm this hypothesis, we performed a computer simulation of the transport of fluorescence photons from the tumor to the surface of the tissue, using the Monte Carlo approach described in Sec. 2. The main result of this simulation is the distribution and absorption of the excitation light within the tissue [Fig. 1(b)], and more interestingly, the radial distribution of the emitted fluorescence light exiting the tissue [Fig. 1(c)]. The fluorescence intensity detected on the surface is highest at the tumor center ($r = 0$ cm), and it decays radially until the radial edge of the tumor [edge is denoted by dashed black lines in Fig. 1(c)]. Beyond the tumor edge, the fluorescence intensity decay becomes approximately exponential [Fig. 1(d)], which is similar to experimental observation [Fig. 3(c)]. For example, at a distance 3 mm beyond the tumor margin, the fluorescence intensity falls to $\sim 40\%$ of its highest value, compared to $\sim 50\%$ in the experiment. This difference is quite likely due to signal saturation in the experiment. The inset in Fig. 1(d) shows that the radial decay of fluorescence fits a photon diffusion model⁴⁰ and clearly suggests that the measured fluorescence beyond the tumor edge is due to diffusion of fluorescence light from within the tumor.

These observations and analyses indicate that the fluorescence light generated in the primary tumor will travel from 3 to 6 mm beyond the edge of the tumor. Thus, the signals outside the tumor are probably not due to ICG that leaks into the surrounding tissues or to tumor cells beyond the margin that absorbed ICG but rather due to diffusion of fluorescence light from the primary tumor. Importantly, the geometry of the surgical environment provides a natural buffer zone that ensures the surgical margins are not too close to the tumor edges.

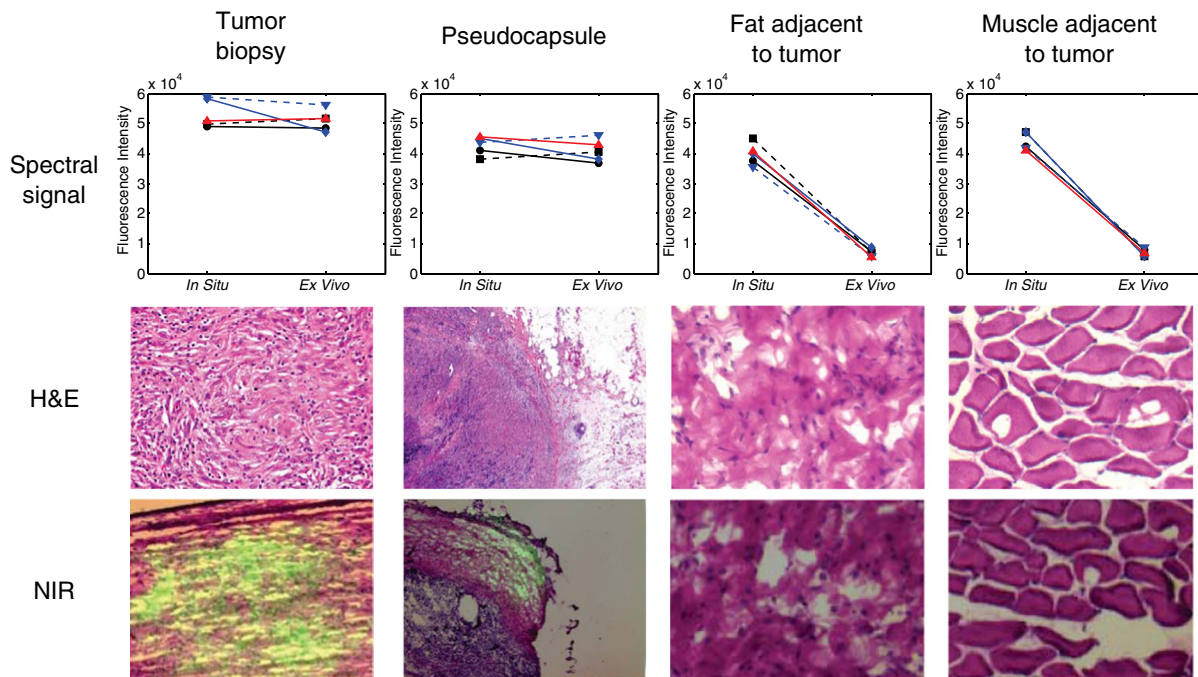


Fig. 6 The NIR signal around the sarcomas typically extended beyond the tumor pseudocapsule into the fat and muscle. The spectral signal from these normal tissues dissipated when the tissue was removed from its *in situ* location. H&E did not demonstrate tumor cells outside the tumor pseudocapsule nor did immunofluorescence identify ICG particles outside the pseudocapsule.

The overestimation of the tumor margin by NIR fluorescence imaging and the establishment of a natural buffer zone for surgical margin is the second significant result of this paper.

3.5 Canine Subject Outcomes

None of the 10 canines that had negative histologic and negative NIR margins (true negatives) have developed local recurrences to date (follow-up 62 to 690 days). The one canine that had positive margin by spectroscopy but no histological evidence of cancer has not developed recurrence to date (in follow-up at 213 days). Of the four canines that had residual disease on both spectroscopy and histopathology, one dog has received full-course (48 gray) definitive radiation treatment. No further surgery has been performed in the remaining three dogs. One of these dogs has had tumor recurrence at the site of the previous surgery. Based on these clinical outcomes, NIR fluorescence imaging and spectroscopy had a sensitivity of 100% (95% confidence interval, CI 0.39 to 1.00) and a specificity of 90.9% (CI 0.54 to 0.99) with a false positive rate of 9.09% (CI 0.01 to 0.70) in detecting residual disease at the surgical margins.

3.6 Pilot Study in Humans with Sarcoma

Two human patients with sarcomas were investigated with NIR fluorescence imaging and spectroscopy. The case of a 57-year-old male patient with an 11-cm mass in the right posterior lateral chest wall (Fig. 7) is described in detail. MRI showed that the lesion was predominantly isointense to the muscle on the T1-weighted pulse sequence and hyperintense on T2-weighted

pulse sequences.¹⁸ FDG-PET demonstrated heterogeneous increased FDG uptake in the tumor with a standardized uptake value of 8.8 (background < 2) that suggests a highly active metabolic tumor. There was no evidence of metastatic disease. The patient was injected with 5 mg/kg of ICG IV 24 h prior to surgery and then underwent a flank incision and resection. During surgery, the primary tumor was exposed and imaged using the NIR imaging system. The fluorescent intensity from the tumor was $49,296 \pm 6549$ counts with an SBR of 10.3 ± 1.5 (average \pm standard deviation).

After the tumor was removed, the surgical wound was examined for fluorescence and no evidence of residual fluorescence was found. Several biopsies were taken, and they confirmed the absence of residual tumor cells. The tumor margins were evaluated on the excised specimen. Similar to the canines, residual fluorescence extended as far as 8 mm from the edges of the tumor, but histologically, no tumor cells were found beyond the capsule of the tumor, although the fluorescence reached as high as 32,198 counts (SBR of 6.7) in the surrounding fat.

The final pathology from the specimen was a 13.0 cm dedifferentiated high-grade (III) pleomorphic sarcoma. The patient had an uneventful postoperative course and remains disease-free after 398 days of follow-up.

The second patient (data not shown) was a 42-year-old male with a 7.2-cm mass in the right axilla that was felt to be involving the first and second rib, scapula, and clavicle. Similar to the first patient, the lesion was metabolically active on ¹⁸FDG-PET and preoperative biopsies suggested a chest wall osteosarcoma. The patient underwent ICG injection and then surgery to remove

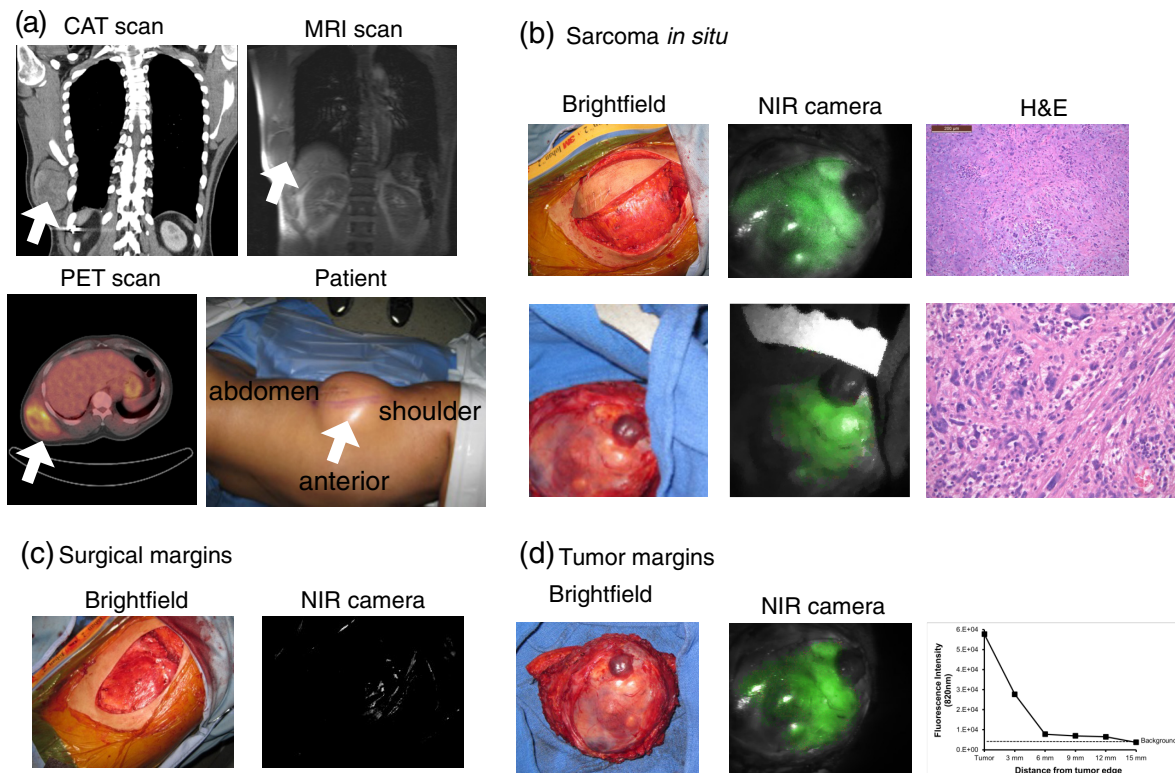


Fig. 7 A 57-year-old male with an 11-cm right lateral flank/chest wall sarcoma underwent surgical resection with NIR imaging. (a) The tumor did not appear to invade into the underlying rib case on T1- and T2-weighted MRI images.¹⁸ FDG-PET demonstrated increased FDG uptake (SUV 8.8). (b) In surgery, the tumor was fluorescent with an S/N ratio of 10.3. (c) After removing the tumor, the wound bed did not have residual tumor cells. (d) The tumor was fluorescent *ex vivo* and the NIR emission signal did extend beyond the pseudocapsule. In follow-up, the patient remains disease free at over 1 year.

the lesion. During surgery, the tumor fluorescent intensity was $55,978 \pm 9875$ counts with an SBR of 8.4 ± 1.9 . After the tumor was removed, the wound was negative for residual fluorescence. *Ex vivo*, the surgical margins did not have cancer cells, including the third rib that abutted the primary specimen. The patient has no local tumor recurrence 2 years postoperatively.

4 Discussion

Local recurrence is an Achilles heel of surgical oncology.⁴¹ With this issue in mind, we have demonstrated that NIR fluorescence imaging and spectroscopy can provide real-time information about tumor margins and surgical margins. The study has several important findings.

First, ICG fluorescence provides contrast for detection of solid cancers. ICG fluorescence signals clearly identified 14/15 canine sarcomas and both human sarcomas. Although ICG (which is a water-soluble probe with a hydrodynamic diameter of 1.2 nm) is a nonspecific fluorophore, it provides excellent contrast via a passive targeting mechanism; ICG-protein complexes (4 to 6 nm) readily leak into and are retained by cancer tissues due to EPR effects.^{1,42} This form of passive targeting does not differentiate tumors from other normal tissue with similarly disordered vascular structures (e.g., inflammation). In this study, only one canine subject had a high concentration of ICG in the surgical margins with no evidence of residual tumor cells. This observation suggests that ICG can accumulate in inflamed tissues, which can be a source of false positives during cancer surgery.⁵ Importantly, for purposes of intraoperative diagnostic imaging, sensitivity for abnormal tissues is significantly more important than specificity.

Second, the investigation explored the margins after tumor removal. NIR fluorescence imaging identified areas of concern in the margins of 5 of the 15 canines studied, three of which were considered to be disease-free by the surgeon. These “suspicious” locations were then interrogated further with NIR fluorescence spectroscopy; the fluorescence spectroscopy device provided excellent negative predictive value, i.e., all margins that were predicted to be disease free had no residual cancer cells. Both human patients that were imaged and found to have no residual disease by spectroscopy showed no histological evidence of tumor cells in the margins and had excellent long-term outcomes. NIR fluorescence imaging and spectroscopy did have one false positive in our series. However, in the surgical setting, it is more important to have a low false negative rate and a high-positive predictive value. False-negative results in this setting imply that residual tumor is present in the wound and could easily cause local recurrence, thereby surgical failure, an outcome which is clearly undesirable. A high-positive predictive value means that there will be far more true positives than false positives; a false positive result would mean that normal tissues would be resected unnecessarily. While resection of additional normal tissue is not typically a major issue, reducing unnecessary resection would improve the precision of the operation and would be desirable for the patient.

A third major idea emerging from the investigation concerns the limitations of NIR fluorescence imaging for identification of surgical margins as a result of diffusion of fluorescence light from the tumor to the surrounding tissues, *in-situ*. NIR fluorescence imaging can overestimate tumor margins; therefore, it provides very conservative surgical guidelines for resection. Our experiments detect a “halo” of fluorescence signal

surrounding a tumor that encircled these sarcomas, extending by ~ 3 mm beyond the tumor. In situations wherein a surgeon requires exact knowledge about the tumor margin, such as near a nerve or critical blood vessel, fluorescence imaging and spectroscopy will have important limitations. We used simulations to examine several possible explanations for the lack of precision in defining the tumor margins and we confirmed that diffusion of NIR fluorescence from the primary tumor to the surrounding tissue (as far as 3 to 6 mm from the tumor capsule) was a critical factor. In situations where precise tumor margins are required, depth sensitivity and accurate three-dimensional localization of ICG fluorescence will become important. Hence, more sophisticated instrumentation and *in-situ* analysis methods may be required, especially given the natural curvatures and irregularities of tumor tissues within the body.

In closing, we acknowledge several limitations. First, our patient population was composed of a limited subset of tumor histologies. The spontaneous canine tumor model was chosen because it mimics the corresponding human disease well, and we are pushing towards more human studies. Second, the optimal time and dose of ICG for purposes of tumor imaging was not determined in a comprehensive study. The numbers we chose were based on preclinical studies, which suggest doses upward of 3 to 5 mg/kg provide superior tissue contrast.⁶ Third, the dynamic range of our measurements was compromised due to saturation of the NIR fluorescence intensity; this effect was especially significant when probing tissues from the tumor core. These saturation effects prevented accurate characterization of the decay of the fluorescence signal from the core to the tumor margins, and they likely led to an underestimation of tumor contrast in the margins. We are currently working to modify the handheld probe and analysis to reduce saturation and better characterize the intratumor fluorescence concentration distribution. We also acknowledge that our procedure to normalize fluorescence to background could be made more rigorous (e.g., normalization with respect to intensity). By holding illumination intensity and integration times constant, however, we ameliorate some of these limitations, especially when only spatial variations in fluorescence are investigated. Finally, we account for variabilities due to different tissue optical properties, by averaging background fluorescence from muscle, fat, and blood vessels [Fig. 5(a)].

In the future, targeted NIR dyes could emerge as attractive for clinical use. Several agents are currently being studied in preclinical models.^{43–45} These contrast agents could help overcome the challenge of nonselective uptake in inflammatory tissue. Receptor-targeted NIR contrast agents will likely accumulate several folds higher in tumor tissues. Nevertheless, although ICG may be nonspecific for some clinical applications, our data do show that intraoperative NIR fluorescence based on ICG contrast is logistically and technically feasible. This system and approach could improve intraoperative information and postoperative decisions, including whether a patient should receive adjuvant radiation therapy or follow-up monitoring and imaging to identify local tumor regrowth.

Acknowledgments

This work was supported by the National Institutes of Health R01 CA163256 (D.H., S.N., and S.S.), (partially by) 5P01 CA087971, P41-EB015893-29, 5R01 NS060653-06 (A.G.Y.), and R03 EB017828 (D.H. and S.S.), the American Heart Association 14POST20460161 (A.B.P.), and an American

Kennel Club Canine Health Foundation ACORN grant (D.H. and S.S.). S.N. is a consultant for SpectroPath, Inc., a startup company to develop advanced instrumentation and nanoparticle contrast agents for image-guided surgery.

References

1. S. Singhal, S. Nie, and M. D. Wang, "Nanotechnology applications in surgical oncology," *Annu. Rev. Med.* **61**, 359–373 (2010).
2. V. S. Klimberg, S. Harms, and S. Korourian, "Assessing margin status," *Surg. Oncol.* **8**(2), 77–84 (1999).
3. A. Vaidya et al., "Intraoperative T staging in radical retropubic prostatectomy: is it reliable?," *Urology* **57**(5), 949–954 (2001).
4. A. Sienko et al., "Frozen section of lung specimens," *Arch. Pathol. Lab. Med.* **129**(12), 1602–1609 (2005).
5. D. Holt et al., "Intraoperative near-infrared imaging can distinguish cancer from normal tissue but not inflammation," *PLoS One* **9**(7), e103342 (2014).
6. B. Madajewski et al., "Intraoperative near-infrared imaging of surgical wounds after tumor resections can detect residual disease," *Clin. Cancer Res.* **18**(20), 5741–5751 (2012).
7. M. M. Haglund, M. S. Berger, and D. W. Hochman, "Enhanced optical imaging of human gliomas and tumor margins," *Neurosurgery* **38**(2), 308–317 (1996).
8. A. Raabe et al., "Near-infrared indocyanine green video angiography: a new method for intraoperative assessment of vascular flow," *Neurosurgery* **52**(1), 132–139 (2003).
9. S. A. Hilderbrand and R. Weissleder, "Near-infrared fluorescence: application to in vivo molecular imaging," *Curr. Opin. Chem. Biol.* **14**(1), 71–79 (2010).
10. S. L. Owens, "Indocyanine green angiography," *Br. J. Ophthalmol.* **80**(3), 263–266 (1996).
11. M. M. Haglund et al., "Enhanced optical imaging of rat gliomas and tumor margins," *Neurosurgery* **35**(5), 930–941 (1994).
12. V. Ntziachristos et al., "Concurrent MRI and diffuse optical tomography of breast after indocyanine green enhancement," *Proc. Natl. Acad. Sci. U. S. A.* **97**(6), 2767–2772 (2000).
13. J. S. Reynolds et al., "Imaging of spontaneous canine mammary tumors using fluorescent contrast agents," *Photochem. Photobiol.* **70**(1), 87–94 (1999).
14. E. Borotto et al., "Detection of the fluorescence of GI vessels in rats using a CCD camera or a near-infrared video endoscope," *Gastrointest. Endosc.* **50**(5), 684–688 (1999).
15. C. Detter et al., "Near-infrared fluorescence coronary angiography: a new noninvasive technology for intraoperative graft patency control," *Heart Surg. Forum* **5**(4), 364–369 (2002).
16. S. L. Troyan et al., "The FLARE™ intraoperative near-infrared fluorescence imaging system: a first-in-human clinical trial in breast cancer sentinel lymph node mapping," *Ann. Surg. Oncol.* **16**(10), 2943–2952 (2009).
17. E. M. Sevick-Muraca et al., "Imaging of lymph flow in breast cancer patients after microdose administration of a near-infrared fluorophore: feasibility study," *Radiology* **246**(3), 734–741 (2008).
18. M. Fujiwara et al., "Sentinel lymph node detection in skin cancer patients using real-time fluorescence navigation with indocyanine green: preliminary experience," *J. Plast. Reconstr. Aesthet. Surg.* **62**(10), e373–e378 (2009).
19. T. Moroga et al., "Thoracoscopic segmentectomy with intraoperative evaluation of sentinel nodes for stage I non-small cell lung cancer," *Ann. Thorac. Cardiovasc. Surg.* **18**(2), 89–94 (2012).
20. O. T. Okusanya et al., "Intraoperative near-infrared imaging can identify pulmonary nodules," *Ann. Thorac. Surg.* **98**(4), 1223–1230 (2014).
21. J. R. van der Vorst et al., "Near-infrared fluorescence-guided resection of colorectal liver metastases," *Cancer* **119**(18), 3411–3418 (2013).
22. A. L. Vahrmeijer and J. V. Frangioni, "Seeing the invisible during surgery," *Br. J. Surg.* **98**(6), 749–750 (2011).
23. M. V. Marshall et al., "Near-infrared fluorescence imaging in humans with indocyanine green: a review and update," *Open Surg. Oncol. J.* **2**(2), 12–25 (2010).
24. J. V. Frangioni, "In vivo near-infrared fluorescence imaging," *Curr. Opin. Chem. Biol.* **7**(5), 626–634 (2003).
25. E. M. Sevick-Muraca, "Translation of near-infrared fluorescence imaging technologies: emerging clinical applications," *Annu. Rev. Med.* **63**, 217–231 (2012).
26. V. Ntziachristos, C. Bremer, and R. Weissleder, "Fluorescence imaging with near-infrared light: new technological advances that enable in vivo molecular imaging," *Eur. Radiol.* **13**(1), 195–208 (2003).
27. O. Okusanya et al., "Small portable interchangeable imager of fluorescence for fluorescence guided surgery and research," *Technol. Cancer Res. Treat.* **14**(2), 213–220 (2015).
28. A. M. Mohs et al., "Hand-held spectroscopic device for in vivo and intraoperative tumor detection: contrast enhancement, detection sensitivity, and tissue penetration," *Anal. Chem.* **82**(21), 9058–9065 (2010).
29. J. Predina et al., "Changes in the local tumor microenvironment in recurrent cancers may explain the failure of vaccines after surgery," *Proc. Natl. Acad. Sci. U. S. A.* **110**(5), E415–E424 (2013).
30. W. Rasband, "Image J," U. S. National Institutes of Health, Bethesda, Maryland, <http://imagej.nih.gov/ij/> (2014).
31. L. Wang, S. L. Jacques, and L. Zheng, "MCML—Monte Carlo modeling of light transport in multi-layered tissues," *Comput. Methods Programs Biomed.* **47**(2), 131–146 (1995).
32. S. L. Jacques, "Monte Carlo simulations of fluorescence in turbid media," in *Handbook of Biomedical Fluorescence*, M. A. Mycek and B. W. Pogue, Eds., Marcel-Dekker, New York (2003).
33. G. Yu et al., "Time-dependent blood flow and oxygenation in human skeletal muscles measured with noninvasive near-infrared diffuse optical spectroscopies," *J. Biomed. Opt.* **10**(2), 024027 (2005).
34. R. Choe et al., "Differentiation of benign and malignant breast tumors by in-vivo three-dimensional parallel-plate diffuse optical tomography," *J. Biomed. Opt.* **14**(2), 024020 (2009).
35. U. Sunar et al., "Noninvasive diffuse optical measurement of blood flow and blood oxygenation for monitoring radiation therapy in patients with head and neck tumors: a pilot study," *J. Biomed. Opt.* **11**(6), 064021 (2006).
36. S. L. Jacques and S. A. Pahl, Oregon Medical Laser Center, Portland, Oregon, <http://omlc.org/spectral/> (2015).
37. H. Maeda et al., "Tumor vascular permeability and the EPR effect in macromolecular therapeutics: a review," *J. Controlled Release* **65**(1–2), 271–284 (2000).
38. H. Maeda, "The link between infection and cancer: tumor vasculature, free radicals, and drug delivery to tumors via the EPR effect," *Cancer Sci.* **104**(7), 779–789 (2013).
39. R. Dagan et al., "The significance of a marginal excision after preoperative radiation therapy for soft tissue sarcoma of the extremity," *Cancer* **118**(12), 3199–3207 (2012).
40. T. Durduran et al., "Diffuse optics for tissue monitoring and tomography," *Rep. Prog. Phys.* **73**(7), 076701 (2010).
41. L. A. Aliperti et al., "Local and systemic recurrence is the Achilles heel of cancer surgery," *Ann. Surg. Oncol.* **18**(3), 603–607 (2011).
42. K. Greish, "Enhanced permeability and retention of macromolecular drugs in solid tumors: a royal gate for targeted anticancer nanomedicines," *J. Drug Target* **15**(7–8), 457–464 (2007).
43. A. G. T. Terwisscha van Scheltinga et al., "Intraoperative near-infrared fluorescence tumor imaging with vascular endothelial growth factor and human epidermal growth factor receptor 2 targeting antibodies," *J. Nucl. Med.* **52**(11), 1778–1785 (2011).
44. M. Hutteman et al., "Intraoperative near-infrared fluorescence imaging of colorectal metastases targeting integrin $\alpha(v)\beta(3)$ expression in a syngeneic rat model," *Eur. J. Surg. Oncol.* **37**(3), 252–257 (2011).
45. L. M. Crane et al., "Intraoperative multispectral fluorescence imaging for the detection of the sentinel lymph node in cervical cancer: a novel concept," *Mol. Imaging Biol.* **13**(5), 1043–1049 (2011).

David Holt is professor of surgery at the University of Pennsylvania School of Veterinary Medicine. He uses spontaneous large animal models to develop and test strategies for intraoperative cancer imaging.

Ashwin B. Parthasarathy is a post-doctoral researcher in physics and astronomy at the University of Pennsylvania. He graduated with a PhD in biomedical engineering from The University of Texas at Austin in 2010, and was subsequently a post-doctoral researcher at Boston University before moving to Penn in 2012. His overall

research goal is the development of optical technology for clinical biomedical applications; including the imaging and monitoring of cerebral blood flow during and after stroke, with laser speckle contrast imaging and diffuse correlation spectroscopy, and intraoperative imaging of tumors.

Arjun G. Yodh is the James M. Skinner professor of science and the director of the laboratory for research on the structure of matter (LRSM) at the University of Pennsylvania. His current interests span fundamental and applied questions in condensed matter physics, medical and bio-physics, and the optical sciences. He has

extensive experience utilizing diffuse optics techniques for monitoring and imaging of hemodynamics in living tissues.

Sunil Singhal is assistant professor in the Department of Surgery at the University of Pennsylvania Perelman School of Medicine. He is director of the thoracic surgery research laboratory, and his laboratory focuses on preventing relapses after cancer surgery. To that end, his laboratory studies molecular imaging to identify sources of local recurrences.

Biographies of the other authors are not available.